Published by SET Publisher

**Journal of Basic & Applied Sciences**

ISSN (online): 1927-5129

# Silica-Supported Sulfuric Acid as Doping Agent in Synthesis of a New Composite of Poly(*o*-methoxyaniline) Under Solid-State Condition

Ilnaz Shariati and Ali Reza Modarresi-Alam*

*Organic and Polymer Research Laboratory, Department of Chemistry, Faculty of Science, And Renewable Energies Research Institute, University of Sistan and Baluchestan, Zahedan, Iran*

**Article Info:**

*Keywords:*
Poly(*o*-methoxyaniline),
composite,
silica-supported sulfuric acid,
solid-state (solvent-free),
doping.

*Timeline:*
Received: July 20, 2021
Accepted: August 24, 2021
Published: August 25, 2021

*Citation:* Shariati I, Modarresi-Alam AR. Silica-Supported Sulfuric Acid as Doping Agent in Synthesis of a New Composite of Poly(o-methoxyaniline) Under Solid-State Condition. J Basic Appl Sci 2021; 17: 115-126.

*DOI:* https://doi.org/10.29169/1927-5129.2021.17.13

**Abstract:**

The objective of this research is the synthesis and characterization of the novel composite of poly(*o*-methoxyaniline)/silica-supported sulfuric acid (POMA-SSSA). The synthesis is done by doping of poly (*o*-methoxyaniline) emeraldine base in the presence of silica-supported sulfuric acid ($SiO_2$-$H_2SO_4$, SSSA) under solid-state (solvent-free) conditions. Herein, poly(*o*-methoxyaniline) emeraldine salt (POMA-SA) is prepared simply by mixing the base form with $H_2SO_4$ in solid-state. The doping process is verified by ultraviolet-visible, Fourier transform infrared spectroscopy and elemental analysis. It is shown that the polymers and composites have maximum doping and the doping counter ion in POMA-SA and POMA-SSSA-bw (before work-up) is $HSO_4^-$ and in the POMA-SSSA-aw (after work-up) is $SO_4^{2-}$. The prepared composites show good conductivity. Scanning electron microscopy (SEM) images show that POMA molecules thoroughly have coated the surface of silica. Moreover, the morphology studies of composites show a smooth surface and sheet-like layer that have covered the particles within the range of 0.5 to 1 µm.

*Corresponding Author
Tel: +98-5433431146
E-mail: modaresi@chem.usb.ac.ir

## 1. INTRODUCTION

In the past three decades, polyaniline (PANI) has been favored by far as an organic, highly tunable and environmentally stable conducting polymer, producible as film and bulk powder with the feasibility of large-scale and low-cost production. PANI has great potential for commercial applications such as corrosion-prevention coatings, antistatic coatings, chemical sensors, batteries, supercapacitors and energy storage [1-3]. However, a number of factors have limited these applications including problems with processability, solubility, and low mechanical strength. Solubility of polyaniline can be improved by amphiphilic substitutions such as alkyl, alkoxy, and sulfonic groups [1]. POMA is one of the most important of these benefited by substitution of methoxy group [4]. Similarly, organic–inorganic composites with various incorporation of two components have gained considerable attention as they have demonstrated very interesting physical features and potential usages [5,6]. Many uses therefore rely on composite structures; a typical substrate that provides the desired mechanical properties, coated with a film of conducting polymer adds the required electrical, optical, and chemical properties. Some of the most frequently used inorganic particles such as metal oxides ($Fe_2O_3$, $Fe_3O_4$, $TiO_2$, $SiO_2$, $WO_3$, ZnO, $SnO_2$) [5-8] and metals (Au, Ni, Ag, Pd, Pt) [9-13] were used for the polyaniline based composites. Among these polymers, the use of silica particles is increasingly growing because of their large porous volume, high specific area, and large mechanical and thermal stability. Silica is an important material since it is widely used in pharmaceutical, electronic packaging and also in the preparation of silica glass, structural ceramics, chromatographic columns, etc. [5,6,14,15].

Polymeric acids such as poly(acrylic acid) and poly(styrene sulphonic acid) that are immobile and not easily displaced from the backbone, were used as a dopant with a PANI backbone to produce electrically conductive emeraldine salt forms [16]. The use of solid acids such as silica sulfuric acid (SSA) and SSSA for synthesizing organic intermediates and fine chemicals have largely gained attention to further research activities [17-19].

Additionally, since significant efforts have been made to find an alternative to organic solvents, a very attractive substitute for these solvents would be solvent–free (solid-state) reactions that are industrially important due to their reduced pollution, low cost, and simplicity in process and handling [17,18,19c,20]. SSA and SSSA can provide this “green chemistry” condition [17-19].

The objective of this research is to expand the application of heterogeneous reagents and solid acids for the development of synthetic methodologies [17-19]. In this way we developed a method for silica modification with conductive polymers such as POMA in the absence of liquid dispersion medium. It is important to note that none of above strategies has yet been reported. Indeed, this paper involves a comprehensive set of strategies; such as green and solvent-free (solid- state) condition, use of solid acids (e. g. SSSA) in replacing conventional acid/base catalysts (protonic acid media).

The resulting composites were characterized and studied by using CHNS, the electrical conductivity measurements, FT-IR and UV-vis spectroscopy. The SEM was also used to study the morphologies of composites.

## 2. EXPERIMENTAL

### 2.1. Materials

Silica particles with the average particle size of 0.2-0.06 mm of mesh 60 were purchased from Merck. It was dried in furnace at 500°C for 24 h before use. All other chemicals and solvents such as HCl, $NH_3$, ammonium persulfate (APS), *m*-cresol (MCR) and dimethyl sulfoxide (DMSO), sulfuric acid ($H_2SO_4$, 98%) and *o*-methoxyaniline from Merck, and KBr powder and *N*-methyl-2-pyrolidinone (NMP) from Fluka were obtained and used as received without further purification. *o*-Methoxyaniline (OMA) was double distilled under vacuum before use.

### 2.2. Chemical Characterization

FT-IR spectra of products were taken on a JASCO spectrum 2000 spectrophotometer in the range of 400-4000 $cm^{-1}$. The samples were prepared in the pellet form using spectroscopic grade KBr powder. The UV-visible spectra of the samples solutions in *N*-methyl-2-pyrolidinone (NMP), *m*-cresol (MCR) and dimethylsulfoxide (DMSO) were recorded using Shimadzu spectrophotometer in the range of 200-1000 nm. Elemental analysis of C, H, N and S was performed on elementar vario EL instrument. The morphologies were investigated with S-360 field emission scanning electron microscope (SEM). The electrical conductivity measurements were carried out

on 1 cm diameter pellets of the samples at 25°C, using a SDY-IV four-probe instrument.

### 2.3. Synthesis

#### *2.3.1. Preparation of Poly(o-methoxyaniline) Emeraldine Base (POMA-EB)*

The polymer emeraldine salt was synthesized similar to the method used by Muttoso and Bulhoes [4c], except equal molar ratio of oxidant to monomer (Ox/Mon=1) was used to increase the reaction yield. Typically 3.69 g (0.03 mol, 3.38 ml) of OMA dissolved in 300 ml of HCl (1M). The solution was cooled at 0 °C. Then 6.84 g (0.03 mol) of ammonium persulfate (APS) was dissolved in 120 ml of HCl (1M) and added dropwise under vigorous stirring to the first solution. The reaction mixture was kept in ice bath (0-5) °C for 2 hours under constant stirring. Dark green sediment was obtained in the amount of 2.31 g. The sediment was filtered and washed with HCl (1M). The prepared salt (POMA-ES) was then converted into its base form by treating with excess of $NH_4OH$ solution (400 ml, 1M) for 12 hours. The 0.88 g of greenish-black precipitate was filtered and washed with $NH_4OH$ solution and dried at room temperature to yield POMA-EB, Scheme **1**.

#### *2.3.2. Synthesis of Silica-Supported Sulfuric Acid (SSSA)*

At first, silica was placed in stove at 500°C for 24 hours before using. Then the active silica (0.12 g) and sulfuric acid (0.022 ml, 98% weight) were ground completely in a mortar [19c], Scheme **2**.

#### *2.3.3. Preparation of Poly(o-methoxyaniline)/Silica-Support Sulfuric Acid Composite (POMA-SSSA)*

The preparation process for POMA-SSSA is shown in Scheme **2**. The SSSA was ground completely in a mortar. After grinding for about 10 minutes, 0.1 g of POMA-EB was added and ground for 30 minutes. The doping was allowed to proceed for 12 hours at room temperature to give POMA-SSSA-bw (before work-up composite). Then 10 ml doubly distilled water (DDW) was added to this dark powder. The product was then filtered and washed with DDW until the filtrate was colorless. After drying at room temperature, the greenish black composite was dried in 50-60 ºC in an oven for 1 hour to give POMA-SSSA-aw (after work-up composite). The yield of POMA-SSSA-aw composite was 53%.

#### *2.3.4. Doped POMA by Sulfuric Acid (98%) (POMA-SA)*

POMA-SA was prepared in the absence of silica. First 0.2 g of POMA-EB was put in the mortar. Then 0.8 mmol (0.044 ml, 98% weight) sulfuric acid was added gradually and ground for 30 minutes. The greenish black solid of POMA-SA was obtained.

## 3. RESULTS AND DISCUSSION

### 3.1. Elementary Analysis (CHNS)

The results of elemental analysis obtained for POMA-SA and POMA-SSSA (bw and aw) are given in Table **1**. According to these results, their doping percentage

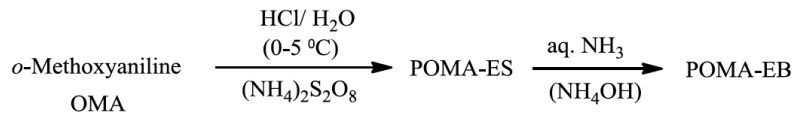


**Scheme 1:** Synthesis of POMA-ES and POMA-EB.

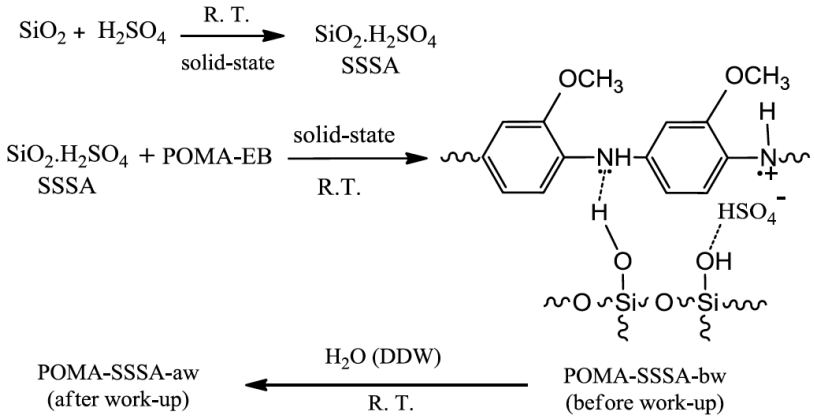


**Scheme 2:** Synthesis of composites POMA-SSSA-bw and –aw.

**Table 1: The Results of the Elemental Analysis (CHNS)**

| | Samples elemental composition (%) | | |
|---|---|---|---|
| | **POMA-SSSA-bw** | **POMA-SSSA-aw** | **POMA-SA** |
| C | 23.14 | 24.88 | 40.73 |
| N | 3.91 | 4.09 | 6.73 |
| S | 5.24 | 2.39 | 9.49 |
| H | 2.53 | 3.11 | 5.12 |
| O | - | - | 37.93 |
| Si+O | 65.18 | 65.54 | - |
| Σ | 100 | 100 | 100 |
| N/S | 1.71 | 3.92 | 1.62 |
| C/S | 11.82 | 27.80 | 11.46 |
| C/N | 6.91 | 7.10 | 7.06 |
| H/C | 1.3 | 1.49 | 1.50 |
| O/S | - | - | 8.01 |
| S/N×100 | 58.42% | 25.52% | 61.64% |
| Experimental formula | $[(C_7H_7NO)_4]^{+2}[(HSO_4)_2]^{-2}$ | $[(C_7H_7NO)_4]^{+2}[SO_4]^{-2}$ | $[(C_7H_7NO)_4]^{+2}[(HSO_4)_2]^{-2}$ |

based on S percentage are 61, 58 and 25 for POMA-SA, POMA-SSSA-bw and POMA-SSSA-aw, respectively.

These results show that the S percentage reached to half value after adding water to POMA-SSSA-bw for generating POMA-SSSA-aw. It seems that the doping percentage for POMA-SSSA-aw decreased and is incomplete. However, UV and FT-IR (next sections) show complete doping. Indeed, significant difference is not observed between their doping by UV and FT-IR. Thus we suggest the sulfate anion ($SO_4^{-2}$) for charge balance of two positive nitrogen atoms on polymer chain instead of $HSO_4^-$ anion in POMA-SA and POMA-SSSA-bw, Scheme **3**. In fact, they have experimental formulas $[(C_7H_7NO)_4]^{+2}[(HSO_4)_2]^{-2}$ for POMA-SA and POMA-SSSA-bw, and $[(C_7H_7NO)_4]^{+2}[SO_4]^{-2}$ for POMA-SSSA-aw. It is reasonable that addition of water converts the $HSO_4^-$ anion to $SO_4^{-2}$ anion that later becomes counter ion of polymer (compare Schemes **2-4**). Therefore, the oxidation state is in accordance with the emeraldine oxidation state that is indicative of maximum doping level i.e. ~50%, in accord with the

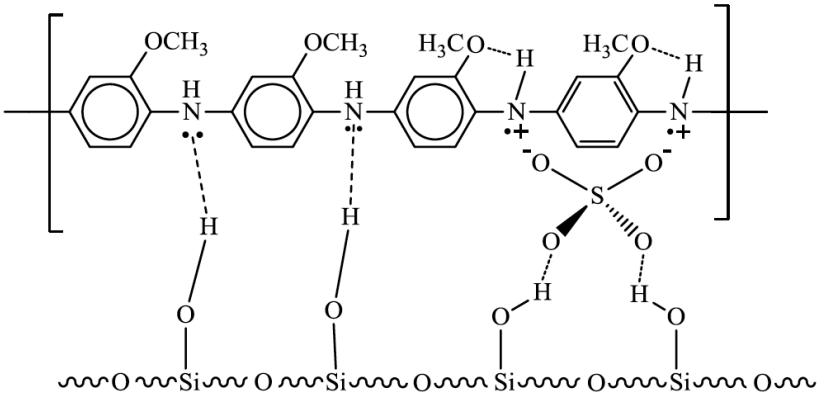

**Scheme 3:** Proposed structure of POMA-SSSA-aw.

$$HSO_4^- + H_2O \longrightarrow SO_4^{-2} + H_3O^+$$

**Scheme 4:** Conversion of $HSO_4^-$ anion to $SO_4^{-2}$ after adding water in work-up for generating POMA-SSSA-aw.

proposed structure in Schemes **2** and **3** for POMA-SSSA-bw and POMA-SSSA-aw, respectively.

### 3.2. FT-IR Spectroscopy

The FT-IR spectroscopy was used for structural characterization of synthesized polymers and composites. Figure **1** shows the FT-IR spectra of silica, POMA-SA and POMA-SSSA (bw and aw) synthesized by solid-state method.

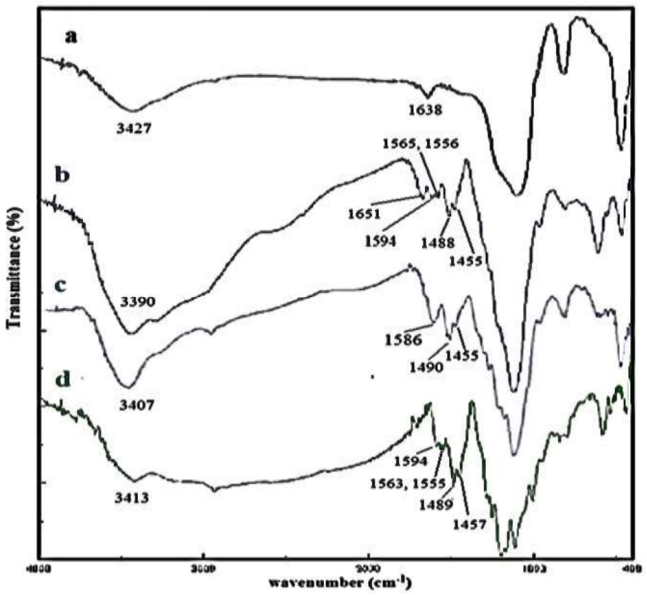


**Figure 1:** FT-IR spectra of a) silica, b) POMA-SSSA-bw, c) POMA-SSSA-aw and d) POMA-SA.

The FT-IR spectrum of the silica exhibits a band at 813 $cm^{-1}$ corresponding to the OH bending of Si–O-H. The band at 973 $cm^{-1}$ is attributed to stretching vibration of Si–OH group. The broad band at 3428 $cm^{-1}$ is attributed to –OH group stretching. The band at 1099 $cm^{-1}$ is assigned to Si–O–Si asymmetric stretching, while Si–O–Si bond rocking is about 466 $cm^{-1}$ [14,15,17-19,21].

The main characteristic peaks of POMA-SA are assigned as the following: the peak at 3413 $cm^{-1}$ due to the N-H stretching vibration suggests the presence of –NH– groups in *o*-anisidine units. The peaks at 1594 and 1563 $cm^{-1}$ are attributed to C=N and C=C stretching modes for the quinoid and the peaks at 1489 $cm^{-1}$ are attributed to C=C stretching modes for benzenoid rings. However, the peak at 1594 $cm^{-1}$ can be attributed to Raman active -C=C- ring stretching vibration. These normally infrared-inactive modes become infrared-active when the protonation induces conformation changes in the polymer chain i.e. when polarons or bipolarons are produced, resulting in symmetry breaking along the chain [1-4,22,23]. The band 1457 $cm^{-1}$ is attributed to the skeletal C=C stretching vibration of the aromatic ring and C–H asymmetric bending of the $OCH_3$ group. The band at 1377 $cm^{-1}$ represents the presence of C–H symmetric bending of the $OCH_3$ group. The band characteristic of the conducting protonated form is observed at 1255 $cm^{-1}$ in the spectrum of this sample. It has been interpreted as corresponding to a $C–N^{+\bullet}$ stretching vibration in the polaron structure [1-4,22]. This peak and the peak at 1563 $cm^{-1}$ for the protonated quinoid establish doping of polymer as well. The S=O stretching of $HSO_4^-$ anion can also contribute to 1255 $cm^{-1}$ [22,24]. The observed shoulder at 1339 $cm^{-1}$ is due to stretching vibration of C-N and/or bending vibration of SOH bond [22-24]. The 1,2,4-trisubstituted ring can also contribute to this band [22]. The peak at 1282 $cm^{-1}$ corresponds to stretching of secondary aromatic amine. The peaks at 1120 and 1173 $cm^{-1}$ is assigned to the plane bending vibration of C–H (modes of N=Q=N, $Q=N^+H–B$ and $B–N^{+\bullet}$ H–B) which is formed during protonation [1,4,22,23]. These bands can also contribute to the asymmetric $SO_3$ stretching of $HSO_4^-$ anion [22,24]. The observed shoulder at 1068 $cm^{-1}$ is attributable to the symmetric $SO_3$ stretching of $HSO_4^-$ anion [22,24]. The bands at 1200 $cm^{-1}$ and 1012 $cm^{-1}$ are related to the asymmetric and symmetric C-O-C stretching of alkyl aryl ether linkage, respectively. The band at 1200 $cm^{-1}$ is also attributed to the phenazine-type ring as well as 1556 $cm^{-1}$ [22].

The bands at 956 and 850 $cm^{-1}$ corresponds to the C-H out-of-plane bending vibration of two adjacent hydrogen atoms on a 1,2,4-trisubstituted ring. This confirms the dominating *para*-coupling of constitutional units in polymer chains [22]. The bands at 887 and 956 $cm^{-1}$ have been attributed to stretching of S-OH in the $HSO_4^–$ counter ion. The bending vibration of O-S-O in $HSO_4^-$ appears at 592 $cm^{-1}$ [22,24].

It is evident from Figures **1b** and **1c** that the FT-IR spectra of the composites (bw and aw) contain contributions from both the $SiO_2$ particles (Figure **1a**) and the POMA-SA (Figure **1d**). However, it is difficult to assign some absorption peaks of the composites because of its overlapping with the characteristic peak of $SiO_2$ particles and POMA-SA. By comparing Figure **1b** and **1c** with Figure **1d**, it is also noted that some POMA peaks in POMA-SSSA-aw are shifted due to interactions with $SiO_2$ particles. For example, the stretching modes of C=N, C=C, and C–N at 1563 $cm^{-1}$, 1489 $cm^{-1}$, and 1282 $cm^{-1}$ all shift to higher

wavenumbers 1586 $cm^{-1}$, 1490 $cm^{-1}$, and 1286 $cm^{-1}$ in POMA-SSSA-aw, respectively. Furthermore, the peak at 1594 $cm^{-1}$ has been removed. Similarly, the peak at 1173 $cm^{-1}$ in POMA-SA, formed upon protonation, also shifts to 1157 $cm^{-1}$ in POMA-SSSA-bw and to 1163 $cm^{-1}$ in POMA-SSSA-aw. However, N–H stretching peak at 3413 $cm^{-1}$ shifts to lower and higher wavenumbers in POMA-SSSA-bw and POMA-SSSA-aw, respectively. These FT-IR absorption changes suggest that the C=N, C=C, and C–N bonds become stronger in POMA-SSSA composites, but the N–H bond depend to various hydrogen bonds. This is probably because of the hydrogen bonding between the surfaces of the electronegative $SiO_2$ particles and the N–H group in the POMA macromolecule, as shown in Schemes **2** and **3**.

Furthermore, the asymmetric stretching of Si-O-Si group for $SiO_2$ at 1099 $cm^{-1}$ shifts to higher wavenumbers 1102 and 1111 $cm^{-1}$ in POMA-SSSA-bw and POMA-SSSA-aw, respectively. This blue-shift indicates an absence of hydrogen bonding interaction between oxygen of Si-O-Si group of $SiO_2$ and -NH group of POMA, but it can show the presence of hydrogen bonding interaction between OH of $SiO_2$ surfaces and -NH group of POMA as showed in Schemes **2** and **3**. The band at 1330 $cm^{-1}$ in the spectrum of POMA-base is shifted to lower wavenumbers 1293 $cm^{-1}$ in POMA-SSSA-bw and 1286 in POMA-SSSA-aw. This red-shift is due to the physicochemical interaction (hydrogen bonding between the C–N group of POMA and -OH of silica) that confirms the suggested structures in Schemes **2** and **3**. This is reasonable easily because of more acidity of silica (OH) rather than amines (NH). The 592 $cm^{-1}$ band due to the bending vibration of O-S-O in $HSO_4^-$ in POMA-SA shifts to 603 $cm^{-1}$ in POMA-SSSA-bw [22,24,25]. This band split into two peaks (615 and 592 $cm^{-1}$) in POMA-SSSA-aw, which indicates a lowering of symmetry in sulfate anion ($SO_4^{2-}$) [22,24,25] and it, then, establishes existence of sulfate anion in POMA-SSSA-aw. The shift of frequency from 672 $cm^{-1}$ in sulfates to 660 $cm^{-1}$ in POMA-SSSA-aw indicates that the sulfate ions in POMA-SSSA-aw are linked with silica by hydrogen bonding, because in general the hydrogen bonding will lower the frequency of the absorption band [24,25]. Therefore, the FT-IR spectra of composites and POMA-SA confirm a presence of $HSO_4^-$ and $SO_4^{2-}$ species along with the polymer chain in POMA-SA, POMA-SSSA-bw and POMA-SSSA-aw, respectively as shown in Schemes **2** and **3**.

The bands at 1210-1310 $cm^{-1}$ are assigned to the C-N stretching of the aromatic amines. The band at 1138 $cm^{-1}$ is the characteristic band of the protonated states. Indeed they have also been hidden under 1104 $cm^{-1}$ peak, and therefore, their interpretation is impossible.

Finally, the presence of quinoid and benzenoid bands clearly show that these polymers and composites are composed of amine and imine units. Looking at the band ratio between the benzenoid and quinoid bands in the FT-IR spectra of composites and POMA-SA in Figure **1** i.e. the band ratio 1564/1480, and comparing this ratio with that of various polyanilines, emeraldine salt (ES) structure is confirmed as shown in Schemes **2** and **3**.

### 3.3. UV-Vis Spectroscopy

Figures **2-5** depict the UV-vis spectra recorded by dissolving POMA-EB, POMA-ES, POMA-SA, POMA-SSSA-bw and POMA-SSSA-aw in NMP, MCR and DMSO and data extracted are given in Table **2**.

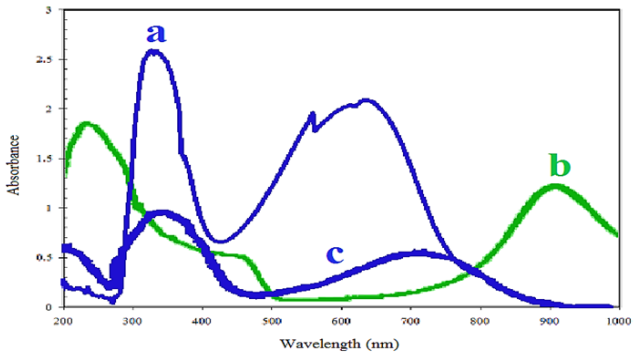


**Figure 2:** UV-vis spectra of a) POMA-EB in NMP (blue), b) POMA-ES in MCR (green) and c) POMA-ES in NMP (blue).

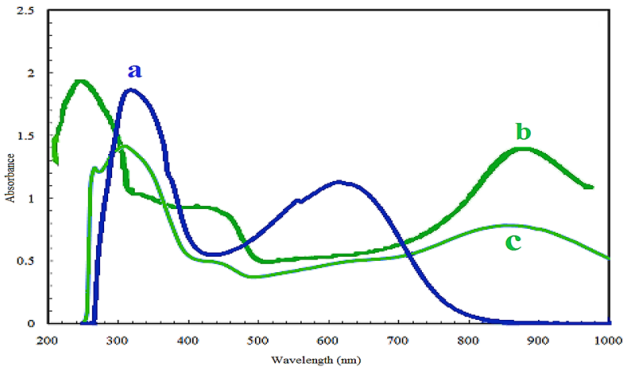


**Figure 3:** UV-vis spectra of POMA-SA in a) NMP (blue), b) MCR (green) and c) DMSO (green).

All samples are blue in NMP and the band at around 305-340 nm is related to π→π* transition of the benzoid rings, while n→π* transition of the benzoid to quinoid rings occurs at about 615-635 nm [1-

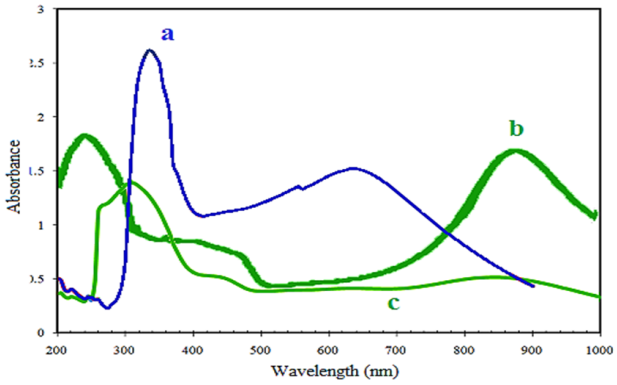


**Figure 4:** UV-vis spectra of POMA-SSSA-bw in a) NMP (blue), b) MCR (green) and c) DMSO (green).

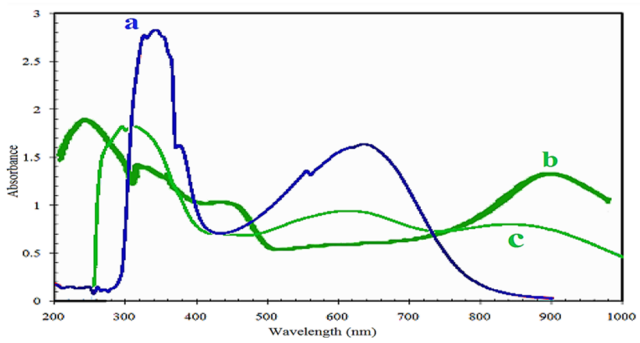


**Figure 5:** UV-vis spectra of POMA-SSSA-aw in a) NMP (blue), b) MCR (green) and c) DMSO (green).

4,17a,19c,23,26-28]. Looking at the blue colored solution of POMA-ES, POMA-SA, POMA-SSSA-bw, POMA-SSSA-aw and the data in Table **2**, it is clear that POMA is in the dedoped emeraldine form in NMP because of both basic nature of the solvent and the limitation of its solubility [26,27]. The doping phenomenon was not observed in NMP even in fully doped POMA-ES. This is verified in literature [1-4, 26, 27] and as shown in Figure **2**.

To demonstrate this matter, the UV-vis absorption spectra of these compounds were recorded in MCR and DMSO as are displayed in Figures **2-5**. In MCR that are clear green solution, they exhibit three characteristic peaks: an absorption peak at ~300 nm representing the transition of the benzenoid ring, and two absorption peaks at ~410 nm and ~850 nm. These last two peaks can be assigned to the polaron band transitions (the metallic polaron band of the conducting form). Indeed, the second and third peaks are attributed to polaron-π* transition and π-polaron transition, respectively. Thus, the presence of these peaks proves that the POMA is obtained in doped state. Furthermore, the absorption at ~850 nm is a characteristic band of the radical cations, formed by head-to-tail coupling of the 2-methoxyanilinium radical cations. In DMSO, composites and polymers also are clear green solution, and have three characteristic peaks similar to MCR. However they have a shoulder at around 600 nm. Furthermore, the peaks at ~850 and ~420 nm have less intensity than MCR. This difference can only be attributed to its difference in geometric structure (or conformation) for the polymer chain. In aprotic solvents such as NMP, DMF, and so on, the polymer chains of PANI and its derivatives have a coil-like conformation [26,27]. The polarons of each tetrameric unit are isolated from each other due to the twist defects between aromatic rings [26,27]. Therefore, the polaron band has little dispersion in energy. In protic solvents especially phenolic compounds such as MCR, the polymer chain of PANI has an expanded coil-like conformation [26,27]. In this more expanded conformation, the twist defects between aromatic rings are removed. The interaction between the adjacent isolated polarons, therefore, becomes stronger, and the polaron band becomes more dispersed in energy (more delocalized). This is probably due to the tendency of MCR to act as a secondary dopant a phenomenon introduced by MacDiarmid [27], and also due to the fact that it promotes the protonation of the polymer chains and hence the conducting phase. On the other hand, since NMP is a highly polar solvent, the solvent-solute interaction would be stronger than that in the *m*-cresol medium. Nonetheless, the C=O group present in NMP

**Table 2: Data of UV-Vis Spectra of POMA-EB, POMA-ES, POMA-SA, POMA-SSSA-bw and POMA-SSSA-aw) in NMP, MCR and DMSO**

| Compound | | NMP | MCR | DMSO |
|---|---|---|---|---|
| POMA-EB | | 627, 310 | 910, 685, 425, 350, 250 | - |
| POMA-ES | | 628, 305 | 871, 410, 242 | - |
| POMA-SA | | 615, 315 | 885, 413, 324, 242 | 850, 615, 425, 310 |
| POMA-SSSA | bw | 635, 340 | 840, 410, 340, 243 | 845, 620, 440, 310, 265 |
| | aw | 635, 340 | 895, 421, 319, 243 | 845, 610, 310 |

interacts more efficiently with the protons over the polymer chains and thereby has a tendency to absorb the protons. Also, it has been reported in the literature that the competing hydrogen bonding between the carbonyl group of NMP and the acid may suppress the protonation of PANI-base, therefore reducing the concentration of the conducting phase at 800 nm [26, 27]. This leads to the disappearance of the conducting phase peak at 800 nm, together with the suppression of the polaronic peak at 420 nm, while an intense peak appears at 600 nm corresponding to the base form of the polymer.

In some reports, peak at 600 nm is observed even in MCR for both POMA and PANI, which indicates the presence of emeraldine base or pernigraniline forms [4j,4k,23]. Thus, since this peak is not seen, POMA-SSSA (bw and aw) is completely in doped state and the emeraldine salt form of POMA.

We infer that DMSO, despite having a higher dielectric constant of (49 D) than NMP (32 D), is not able to form hydrogen bonding and cannot deprotonate polymer similar to NMP. In fact DMSO acts between NMP and MCR.

The effect of $SiO_2$ component on the polaron peaks of the POMA-SA component can also be observed from the UV-vis spectra. The polaron absorption peak centered at 845 nm of composites (bw and aw) exhibit a blue-shift phenomenon as compared with that of POMA-SA. This indicates that the stronger bonding strength of composite appeared after incorporating $SiO_2$, which would restrict delocalization of polarons or electrons along POMA subchains. These results that are consistent with last sections finding are also consistent with results presented in Schemes **1-3**. Therefore, this implies that $SiO_2$ has an effect on the doping level of conducting POMA.

### 3.4. Conductivity

The conductivities of POMA-ES, POMA-EB, POMA-SA, and composites (bw and aw) obtained by solid-state condition is listed in Table **3**.

As indicated in Table **3**, in doped form, all the polymer powders were conductive, whereas the undoped state of the polymers had a low conductivity level.

The electrical conductivity depends mainly on the number and mobility of the charge carriers and can be correlated with the chemical composition and morphology in evaluating the electrical properties of polymers. The electrical conductivity of PANI is higher than that of the POMA and POMA-SSSA (bw and aw). Generally, conducting polymers with substituents on their frameworks show lower conductivities compared with those of the original PANI. The presence of substituents in the polymer chain can induce some non-planer conformations that decrease the conjugation along the backbone [27,30]. Furthermore, bonding of the side group, the distance between the two main chains increases, and this makes the interchain polaron or bipolaron doping more difficult. It is reported that the conductivity of PANI and its derivatives depends on the degree of doping, oxidation state, particle morphology, crystallinity, inter-or intrachain interactions, molecular weight, etc. [1-4,23,30].

Silica is a type of insulator, that when combined with conductive POMA, forms new interactions. The silica particles are arranged disorderly, and many POMA particles were hindered by the silica in the formation of good conductive approaches.

### 3.5. Scanning Electron Microscopy (SEM)

The SEM images of $SiO_2$ particles, POMA-EB, POMA-SA, and POMA-SSSA-bw, and POMA-SSSA-aw are shown in Figures **6-9**.

It can be seen from Figure **6** that the original spherical commercial $SiO_2$ particles were aggregated with an irregular shape. This can be attributed to the high surface energy of particles. As shown in Figures **7** and **8**, it can be observed the POMA-EB and the POMA-SA particles appear as large globular agglomerates with smooth surface. However, a different appearance was observed for the POMA-SSSA composites particles (Figures **9a** and **b**). It is observed from the images that

**Table 3: The Conductivities of POMA (ES and EB), POMA-SA, PANI (ES and EB) and Composites (bw and aw)**

| Compound | POMA-ES (HCl) | POMA-EB [28] | PANI-ES (HCl) [29] | PANI-EB [29] | POMA-SA | POMA-SSSA-bw | POMA-SSSA-aw |
|---|---|---|---|---|---|---|---|
| Conductivity (S/cm) | $3.97\times10^{-3}$ | $<10^{-5}$ | 4.37 | $6\times10^{-11}$ | 0.034 | $5.19\times10^{-3}$ | $1.05\times10^{-3}$ |

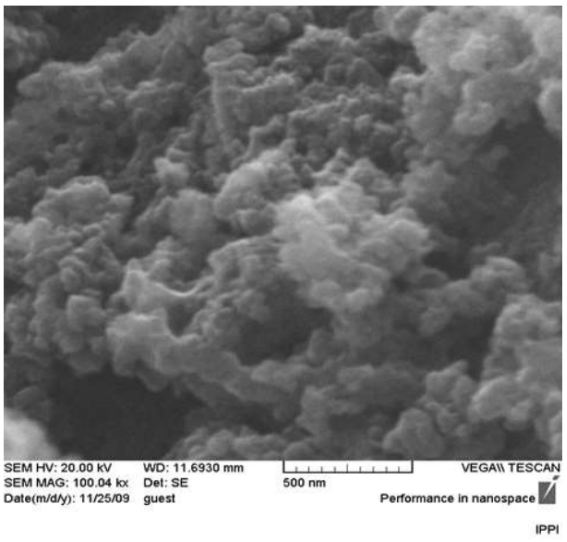


**Figure 6:** SEM image of silica.

the POMA-SSSA (Figures **9a** and **9b**) particles were sheet-like, with particle sizes in the range of 0.5-1 μm. Spheres having a diameter below 200 nm have been observed to accompany composite particles. Comparing the spherical $SiO_2$ particles and composite particles, it can be found that $SiO_2$ particles have a higher surface energy and a stronger tendency toward aggregation. In fact, small discontinuous particles of synthesized polymer can be seen at the surface of silica particles.

The SEM images suggest that POMA molecules, which cannot be incorporated into the pores of silica has consequently coated the surface of silica thoroughly. Furthermore, if POMA molecules had penetrated into silica pores it would have shown less doping level than 50% as demonstrated for MMT and PANI by Yoshimoto and coworkers [31]. The reason why PANI is located outside the clay platelets (MMT) is that it is readily doped as formed, compared with that intercalated into the nanointerlamellar spaces [31].

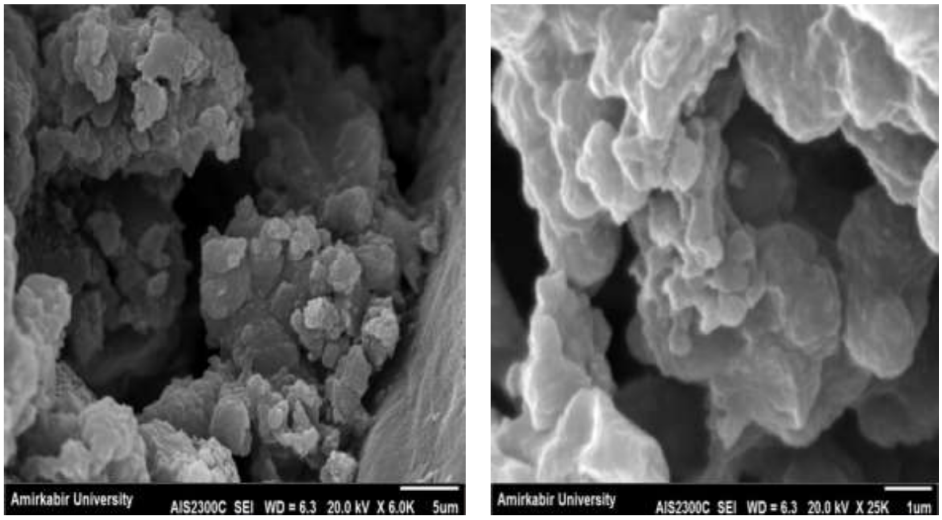


**Figure 7:** SEM image of POMA-EB in two various magnitudes.

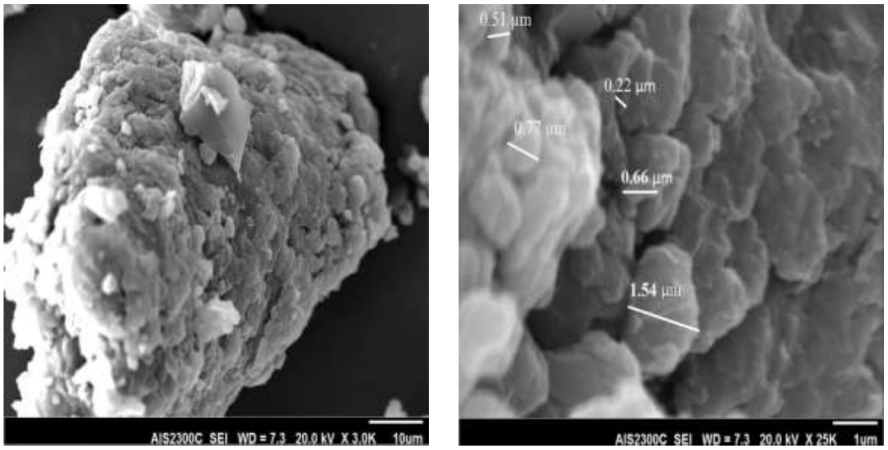


**Figure 8:** SEM image of POMA-SA in two various magnitudes.

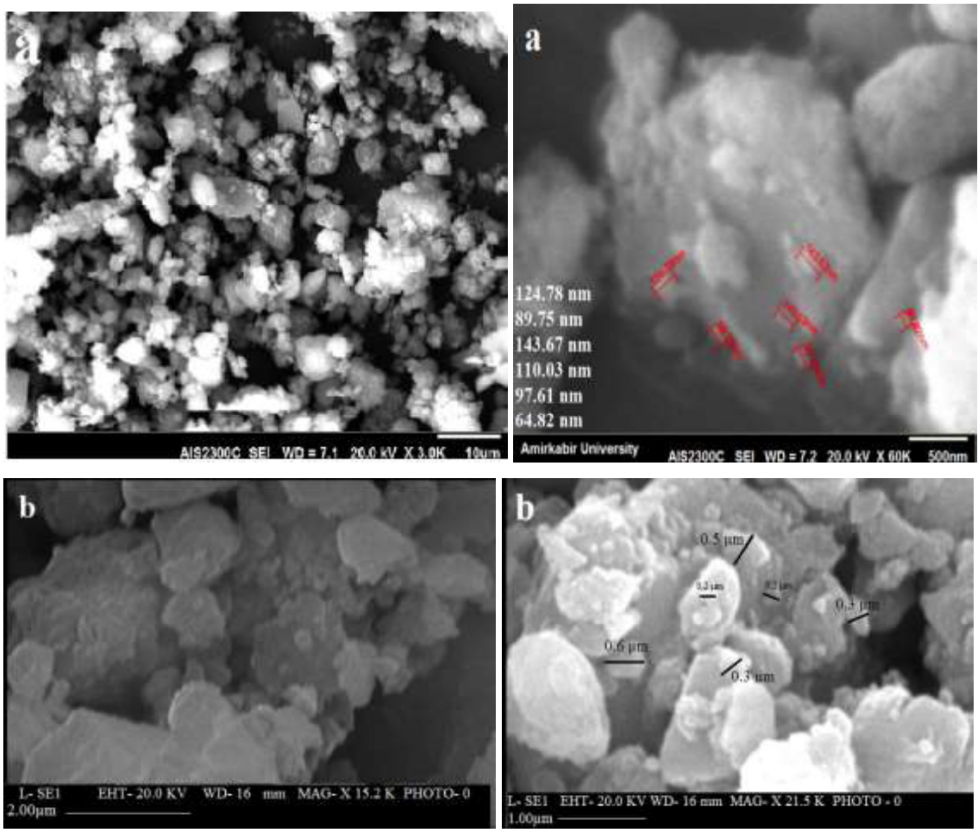


**Figure 9:** SEM images of composites **a**) POMA-SSSA-bw and **b**) POMA-SSSA-aw in two various magnitudes.

## 4. CONCLUSIONS

In this work, composites of POMA-SSSA by doping of POMA-EB in the presence of SSSA under solid-state (solvent-free) condition were synthesized and interactions among POMA and SSSA components were revealed by FT-IR and UV-vis spectra. The results of the spectra analyses show that the composites are not a simple blend of POMA with $SiO_2$ particles. An interaction exists at the interface of $SiO_2$ particles and POMA. We use a solid acid (SSSA) in replacing conventional acid/base catalysts (protonic acid media). The morphology of polymers and composites was determined by SEM images. The SEM images suggest that POMA molecules coated the surface of silica thoroughly. The synthesis method we used here is very simple in comparison with methods used in previous studies, and thus has a significant potential for commercialization of the technology. Further studies on synthesis of other conductive polymers composites are in progress.

## ACKNOWLEDGEMENTS

The authors acknowledge the financial support of grant from the Graduate Council of University of Sistan and Baluchestan.

## REFERENCES

[1] a) Freund MS, Deore B. Self-Doped Conducting Polymers, Canada: John Wiley. 2007. b) Wallace G, Kane-Maguire LAP, Teasdale PR. Conductive Electroactive Polymers, 3th ed. CRC Press: Taylor & Francis Group, 2009. c) Eftekhari A. Nanostructured Conductive Polymers. John wiley & Sons Ltd. 2010.

[2] Bhadra S, Khastgir D, Singha NK, Leeb JH. Progress in preparation, processing and applications of polyaniline. Prog Polym Sci 2009; 34: 783-810. https://doi.org/10.1016/j.progpolymsci.2009.04.003

[3] Kang ET, Neoh KG, Tan KL. Polyaniline: A polymer with many interesting intrinsic redox states. Prog Polym Sci 1998; 23: 277-324. https://doi.org/10.1016/S0079-6700(97)00030-0

[4] a) Macinnes D, Funt BL. Poly-o-methoxyaniline: A new soluble conducting polymer. Synth Met 1988; 25: 235-242. b) Gupta MC, Umare SS. Studies on poly (o-methoxyaniline), Macromol 1992; 25: 138-142. c) Mattoso LHC, Bulhoes LOS. Synthesis and characterization of poly(o-anisidine) films. Synth Met 1992; 52: 171-181. d) Jamal R, Abdiryim T, Ding Y, Nurulla I. Comparative studies of solid-state synthesized poly(o-methoxyaniline) doped with organic sulfonic acids. J Polym Res 2008; 15: 75-82. e) Jamal R, Abdiryim T, Nurulla I. Comparative studies of solid state synthesized poly(o-mehoxy anilne) and Poly(o-toluidine). Polym Adv Technol 2008; 19: 1461-1466. f) Hasik M, Wenda E, Paluszkiewicz C, Bernasik A, Camra J. Poly(o-methoxyaniline)-palladium systems: Effect of preparation conditions on physico-chemical properties. Synth Met 2004; 143: 341-350. g) Kuramoto N, Takahashi Y, Nagai K, Koyama K. Electrorheological properties of poly(o-anisidine) and poly(o-anisidine)-coated silica suspensions. React Funct Polym 1996; 30: 367-373. h) Inamuddin, Ismail YA. Synthesis and

characterization of electrically conducting poly-o-methoxyaniline Zr(1V) molybdate Cd(II) selective composite cation-exchanger. Desalination 2010; 250: 523-529. i) Malmonge LF, Mattoso LHC. Thermal analysis of conductive blends of PVDF and poly(o-methoxyaniline). Polym 2000; 41: 8387-8391. j) Sui J, Zhang L, Peng H, Travas-Sejdic J, Kilmartin PA. Self-assembly of poly(o-methoxyaniline) hollow nanospheres from a polymeric acid solution. Nanotechnology 2009; 20: 415606. k) Kulkarni MV, Viswanath AK. Spectroscopic, thermal and electrical properties of sulphonic acids doped poly(o-anisidine) and their application as humidity sensor. Sen. Actuators B 2005; 107: 791–797. l) Jiang J, Ai LH, Liu AH. A novel poly(o-anisidine)/$CoFe_2O_4$ multifunctional nanocomposite: preparation, characterization and properties. Synth Met 2010; 160: 333-336. https://doi.org/10.1016/j.synthmet.2009.10.032

[5] Zou H, Wu S, Shen J. Polymer/silica nanocomposites: Preparation, characterization, properties, and applications. Chem Rev 2008; 108: 3893-3957. https://doi.org/10.1021/cr068035q

[6] a) Anand J, Palaniappan S, Sathyanarayana DN. Conducting Polyaniline Blends and Composites. Prog Polym Sci 1998; 23: 993-1018. b) Pud A, Ogurtsov N, Korzhenko A, Shapoval G. Some aspects of preparation methods and properties of polyaniline blends and composites with organic polymers. Prog Polym Sci 2003; 28: 1701-1753. https://doi.org/10.1016/j.progpolymsci.2003.08.001

[7] Avvaru NR, Detacconi NR, Rajeshwar K. Compositional Analysis of Organic-inorganic Semiconductor Composites. Analyst 1998; 123: 113-116. https://doi.org/10.1039/a703197a

[8] Wan M, Zhou W, Li J. Composite of polyaniline containing iron oxides with nanometer size. Synth Met 1996; 78: 27-31. https://doi.org/10.1016/0379-6779(95)03562-1

[9] Sivakumar M, Gedanken A. A Sonochemical method for the synthesis of Polyaniline and Au-polyaniline composites using $H_2O_2$ for enhancing rate and yield. Synth Met 2005; 148: 301-306. https://doi.org/10.1016/j.synthmet.2004.10.009

[10] Oliveira MM, Castro EG, Canestraro CD, Zanchet D, Uqarte D, Roman LS, Zarbin AJG. A simple two-phase route to silver nanoparticles/polyaniline structures. J Phys Chem B 2006; 110: 17063-17069. https://doi.org/10.1021/jp060861f

[11] Houdayer A, Schneider R, Billaud D, Ghanbaja J, Lambert J. New polyaniline/Ni(0) nanocomposites: synthesis, characterization and evaluation of their catalytic activity in Heck couplings. Synth Met 2005; 151: 165-174. https://doi.org/10.1016/j.synthmet.2005.04.003

[12] Wang J, Neoh KG, Kang ET. Preparation of Nanosized Metallic Particles in Polyaniline. J Colloid Interface Sci 2001; 239: 78-86. https://doi.org/10.1006/jcis.2001.7576

[13] Pillalamarri SK, Blum FD, Tokuhiro AT, Bertino MF. One-pot Synthesis of Polyaniline-Metal Nanocomposites. Chem Mater 2005; 17: 5941-5944. https://doi.org/10.1021/cm050827y

[14] Parida SK, Dash S, Patel S, Mishra BK. Adsorption of organic molecules of silica surface. Adv Colloid Interface Sci 2006; 121: 77-110. https://doi.org/10.1016/j.cis.2006.05.028

[15] Zhuravlev LT. The surface chemistry of amorphous silica. Zhuravlev model, Colloids. Surf A 2000; 173: 1-38. https://doi.org/10.1016/S0927-7757(00)00556-2

[16] a) Kuo CW, Wen TC. Dispersible polyaniline nanoparticles in aqueous poly(styrenesulfonic acid) via the interfacial polymerization route. Europ Polym J 2008; 44: 3393-3401. b) Costa LC, Rubinger CPL, Martins CR. Dielectric and morphological properties of PAni-DBSA blended with polystyrene sulfonic acid. Synth Met 2007; 157: 945-950. c) Kim SJ, Lee NR, Yi BJ, Kim SI. Synthesis and Characterization of Polymeric Acid-Doped Polyaniline Interpenetrating Polymer Networks. J Macrom Sci Part A: Pure Appl Chem 2006; 43: 497-505. d) Kulkarni MV, Viswanath AK, Khanna PK. Synthesis and Characterization of Conducting Polyaniline Doped with Polymeric Acids. J Macrom Sci Part A: Pure Appl Chem 2006; 43: 759-771. e) Kulkarni MV, Viswanath AK, Marimuthu R, Seth T. Spectroscopic, transport, and morphological studies of polyaniline doped with inorganic acids, Polym. Eng Sci 2004; 44: 1676-1681. f) Athawale AA, Kulkarin MV, Chabukswar VV. Studies on chemically synthesized soluble acrylic acid doped polyaniline. Met Chem Phys 2002; 73: 106-110. g) Fu Y, Weiss RA. Proton antion of polyaniline with lightly sulfonated polystyrene. Synth Met 1997; 84: 103-104. h) Liao YH, Levon K. Doping of polyaniline with polymeric dopants in solid state, gel state and solutions. Polym Adv Technol 1995; 6: 47-57. https://doi.org/10.1002/pat.1995.220060107

[17] a) Modarresi-Alam AR, Pakseresht M, Solaimani M, Farzaneh Jobaneh E, Beladi Mousavi M, Pashaei M, Fathipour F, Azaroun M, Zafari S, Movahedifar F, Dindarloo Inaloo I, Faridkia B. Preparation and Characterization of New Nanocomposites of Polyaniline by *in situ* Polymerization and Doping of Aniline in the Presence of Nanosilica Sulfuric Acid under Solvent-Free Condition. In: Proceedings Inter Conf Nanotechnol: Fundamentals and Applications. (Ottawa Ontario Canada4-6 August) 2010; pp. 1-8. b) Khamooshi F, Modarresi-Alam AR. Solvent-free preparation of arylaminotetrazole derivatives using aluminum(III) hydrogensulfate as an effective catalyst. Chin Chem Lett 2010; 21: 892-896. c) Modarresi-Alam AR, Nasrollahzadeh M, Khamooshi F. Solvent-free preparation of primary carbamates using silica sulfuric acid as an efficient reagent, ARKIVOC xvi 2007; 238-245. https://doi.org/10.3998/ark.5550190.0008.g23

[18] Salehi P, Zolfigol MA, Shirini F, Baghbanzadeh M. Silica sulfuric acid and silica chloride as efficient reagents for organic reactions. Curr Org Chem 2006; 10: 2171-2189. https://doi.org/10.2174/138527206778742650

[19] a) Riego JM, Sedin Z, Zaldivar JM, Marziano NC, Tortato C. Sulfuric Acid on Silica-gel: an Inexpensive Catalyst for Aromatic Nitration, Tetrahedron. Lett 1996; 37: 513-516. b) Maleki B, Keshvari Shirvan H, Taimazi F, Akbarzadeh E. Sulfuric Acid Immobilized on Silica Gel as Highly Efficient and Heterogeneous Catalyst for the One-Pot Synthesis of 2,4,5-Triaryl-1H-imidazoles. Int J Org Che 2012; 2: 93-99. c) Modarresi-Alam AR, Irandoost B, The In-Situ Copolymerization of Aniline and *o*-Toluidine in the Presence of Nanosilica-Supported Sulfuric Acid Under Solvent-Free Condition. In: Proceedings of ICNS5 Conference. (Kish Island Iran March) 2014; pp.1257-1259. https://doi.org/10.1016/0040-4039(95)02174-4

[20] a) Stejskal J, Sapurina I, Trchova M, Prokes J, Krivka I, Tobolkova E. Solid-state protonation and electrical conductivity of polyaniline. Macromol 1998; 31: 2218-2222. b) Gong J, Cui XJ, Xie ZW, Wang SG, Qu LY. The solid-state synthesis of poly- aniline/H4SiW12CO40 materials. Synth Met 2002; 129: 187-192. c) Huang J, Moore JA, Acquaye JH, Kaner RB. A mechanochemical route to the conducting polymer polyaniline, Macromol. 2005; 38: 317-321. d) Yoshimoto S, Ohashi F, Kameyama T. Characterization and thermal degradation studies on polyaniline-intercalated montmorillonite nanocomposites prepared by a solvent-free mechanochemical route. J Polym Sci Part B: Polym Phys. 2005; 43: 2705-2714. e) Zhou CF, Du XS, Liu ZW, Ringer SP, Mai YW. Solid phase mechanochemical synthesis of polyaniline branched nanofibers. Synth Met 2009; 159: 1302-1307. f) Bhadra S, Kim NH, Rhee KY, Lee JH. Preparation of nanosize polyaniline by solid-state polymerization and determination of crystal structure. Polym Int 2009; 58: 1173-1180. g) Sedenkova I, Konyushenko EN, Stejskal J, Trchova

M, Prokes J, Solid-state oxidation of aniline hydrochloride with various oxidants. Synth Met 2011; 161: 1353-1360. h) Ubul A, Jamal R, Rahman A, Awut T, Nurulla I, Abdiryim T. Solid-state synthesis and characterization of polyaniline/multi-walled carbon nanotubes composite. Synth Met 2011; 161: 2097-2102.
https://doi.org/10.1016/j.synthmet.2011.07.027

[21] Musić S, Filipović-Vinceković N, Sekovanić L. Precipitation of amorphous SiO2 particles and their properties. Braz J Chem Eng 2011; 28: 89-94.
https://doi.org/10.1590/S0104-66322011000100011

[22] Trchová M, Stejskal J. Polyaniline: The infrared spectroscopy of conducting polymer nanotubes. Pure Appl Chem 2011; 83:1803-1817.
https://doi.org/10.1351/PAC-REP-10-02-01

[23] Kulkarni MV, Viswanath AK, Marimuthu R, Seth T. Spectroscopic, transport, and morphological studies of polyaniline doped with inorganic acids, Polym. Eng Sci 2004; 44: 1676-1681.
https://doi.org/10.1002/pen.20167

[24] Yacovitch TI, Wende T, Jiang L, Heine N, Meijer G, Neumark DM, Asmis KR. Infrared Spectroscopy of Hydrated Bisulfate Anion Clusters: $HSO_4^-(H_2O)_{1-16}$. J Phys Chem Lett 2011; 2: 2135–2140.
https://doi.org/10.1021/jz200917f

[25] Adler HH, Kerr PF. Variations in Infrared Spectra, Molecular Symmetry and Site Symmetry of Sulfate Minerals. Am Mineral 1965; 50: 32-147.

[26] Xis Y, Wiesinger JM, MacDiarmid AG, Epstein AJ. Camphorsulfonic Acid Fully Doped Polyaniline Emeraldine Salt: Conformations in Different Solvents Studied by an Ultraviolet/Visible/Near-Infrared Spectroscopic Method. Chem Mater 1995; 7: 443-445.
https://doi.org/10.1021/cm00051a002

[27] MacDiarmid AG, Epstein AJ. The concept of secondary doping as applied to polyaniline. Synth Met 1994; 65: 103-116.
https://doi.org/10.1016/0379-6779(94)90171-6

[28] Ozdemir C, Can HK, Colak N, Guner A. Synthesis, Characterization, and Comparison of Self-Doped, Doped, and Undoped Forms of Polyaniline, Poly(oanisidine), and Poly[aniline-co-(o-anisidine)]. J Appl Polym Sci 2006; 99: 2182-2192.
https://doi.org/10.1002/app.22718

[29] Stejskal J, Gilbert RG. Polyaniline Preparation of a conducting polymer (IUPAC Technical Report), Pure. Appl Chem 2002; 74: 857-867.
https://doi.org/10.1351/pac200274050857

[30] Zaidi NA, Foreman JP, Tzamalis G, Monkman SC, Monkman AP. Alkyl Substituent Effects on the conductivity of Polyaniline. Adv Funct Mater 2004; 14: 479-486.
https://doi.org/10.1002/adfm.200305488

[31] Yoshimoto S, Ohashi F, Kameyama T. Zero-order kinetics of the thermal degradation of polypropylene/clay nanocomposites, J Polym Sci Part B: Polym Phys 2005; 43: 2705–2714.
https://doi.org/10.1002/polb.20561